Experimental Observation of Microtearing Modes in a Toroidal Fusion Plasma

M. Zuin, S. Spagnolo, I. Predebon, F. Sattin, F. Auriemma, R. Cavazzana, A. Fassina, E. Martines, R. Paccagnella, M. Spolaore, and N. Vianello

Consorzio RFX, Associazione EURATOM-ENEA sulla Fusione, Padova 35127, Italy

(Received 24 May 2012; published 30 January 2013)

Experimental evidences of short wavelength electromagnetic modes are found in the reversed-field-pinch configuration device RFX-mod by means of in-vessel magnetic probes. The modes are revealed during the helical states of the plasma. Their amplitude is well correlated to the electron temperature gradient strength in the core. On the basis of linear gyrokinetic calculations we interpret these instabilities as microtearing modes.

DOI: 10.1103/PhysRevLett.110.055002 PACS numbers: 52.35.Qz, 52.35.Ra, 52.65.Tt, 52.70.Ds

The reversed-field-pinch (RFP) device has nowadays achieved the quasisingle helicity (QSH) scenario as its standard way of operation. This magnetic configuration features a central plasma volume with good magnetic surfaces, partial but effective suppression of the magnetic chaos produced by large-scale tearing modes, and the appearance of transport barriers [1,2]. There is thus growing awareness that microturbulence (with wavelength of the order of a few ion Larmor radii ρ_i) might be invoked as responsible for a non-negligible level of transport beyond collisional limits, as for the other classes of toroidal fusion devices.

In contrast to the enormous body of theoretical work on microturbulence in fusion plasmas, the number of experimental investigations is fairly limited, due to the difficulties in performing measurements at very small length and time scales. Most proofs about the existence and role of the microturbulence are indirect inferences from measurements of large-scale quantities (profiles, fluxes, etc.), and need a number of supplementary hypotheses to link the micro- and the macroscales [3–6]. In this Letter we provide *direct* observations of the presence of small-scale electromagnetic modes in the plasma core. Experimental data are compared with linear gyrokinetic calculations and allow these fluctuations to be interpreted as a signature of the microtearing modes [7,8]; the results shown would make the present work the first instance of a direct evidence for these modes in a laboratory plasma, not just RFP.

The experimental activity has been performed on RFX-mod, the largest operating RFP device ($R = 2$ m and $a = 0.46$ m major and minor radius) [9]. The measurements are carried out by means of a system of in-vessel probes located at the wall, capable of detecting magnetic fluctuations with high time and space resolution: frequencies up to 5 MHz and wavelengths of the order of few centimeters, both in the poloidal and the toroidal directions, are achieved. Clusters of three axial magnetic coils are used, measuring the time variation of the magnetic field along the three spatial dimensions; i.e., $\dot{b}_r$, $\dot{b}_\theta$, and $\dot{b}_\phi$, are (r, θ, ϕ) the usual radial, poloidal, and toroidal coordinates, respectively [10]. In the RFP the B_θ and B_ϕ components of the equilibrium magnetic field are comparable at midradius, while $B_\phi \simeq 0$ in the edge. This makes the $\dot{b}_\phi$ and $\dot{b}_r$ signals more affected than $\dot{b}_\theta$ by long-wavelength instabilities resonant in the edge of the plasma, such as tearing and resistive g modes [11]. In this Letter, we will thus focus on the analysis of the $\dot{b}_\theta$ signals, showing that they are related to $b_\perp$ fluctuations resonant in the core.

Signals recorded by a single coil appear as in the spectrogram (frequency spectrum versus time) of Fig. 1. Overplotted is the time evolution of the toroidal magnetic field fluctuation $b_\phi^{(m=1,n=7)}$ at the edge, with m and n poloidal and toroidal mode numbers. It shows the typical

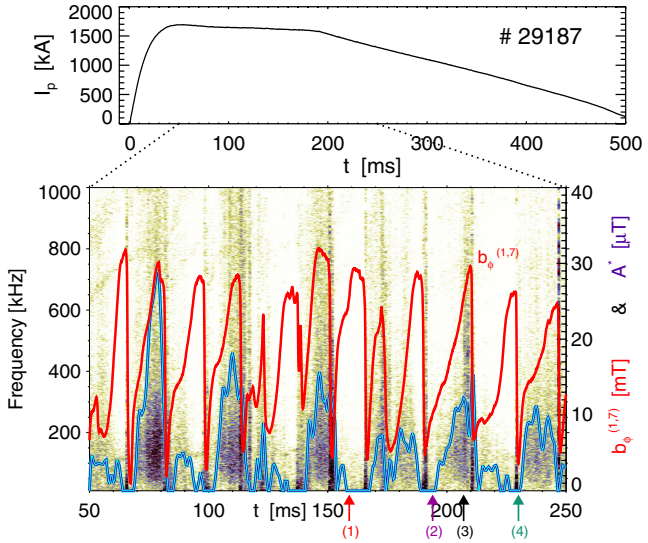

FIG. 1 (color online). Top: plasma current I_p time trace; bottom: spectrogram of a b_θ signal during the flat-top phase of the discharge. The red line is the time trace of $b_\phi^{(1,7)}$ at the edge (y axis on the right-hand side, in mT). The blue line is the estimated amplitude of the high-frequency quasicoherent activity, A^* (y axis on the right-hand side, in μT).

recurrent transitions from the chaotic multiple helicity (MH) state to the QSH state, characterized by a large amplitude of this mode over all the others [12–14]. When $b_\phi^{(1,7)}$ exceeds a certain value, the magnetic field spontaneously reorganizes from an axisymmetric equilibrium with a helical perturbation to a genuine helical equilibrium with better conserved flux surfaces, the so-called single helical axis (SHAx) state [13,15,16].

The spectrogram appears extremely rich, with a spectral density content that varies with time, following the pattern of the tearing mode activity. In particular, we identify three distinct phases. The violet arrow points to a MH phase immediately following a crash of the dominant mode. The corresponding spectrum is shown in Fig. 2(a): it features a smooth decaying trend up to about 600 kHz (at larger frequencies coherent peaks due to Alfvén eigenmodes appear [17]). During the crash the fluctuation amplitude is greatly enhanced in the lowest frequencies range, signature of a global reconnecting rearrangement of the magnetic configuration, producing a broad spectrum of incoherent fluctuations [green arrow and curve in Figs. 1 and 2(a)] [14,18]. The cause of the crash and back-transition QSH → MH is still an open issue in RFP physics.

We are mainly interested in the QSH phases that appear to be characterized by two different phenomenologies: the red curve features a spectrum not dissimilar to that of the MH phase, whereas the black curve exhibits a large broad peak centered around 150 kHz, evidence of quasicoherent electromagnetic activity. In order to disentangle this peak from the background, we have first fitted the latter by a power law curve [$f^{-\alpha}$, with f the frequency, shown by a dashed line in Fig. 2(a)]. The difference between the total signal and this curve, integrated over all the frequency range, yields an estimate A^* of the amplitude of the quasicoherent component.

The time evolution of A^* has been finally overplotted in Fig. 1 (blue line). Good time correlation is found with the behavior of the dominant MHD mode: A^* noticeably increases during the QSH phases, although there are also some counterexamples: these cases correspond to the red curve in Fig. 2(a). Closer analysis of the data shows that a necessary condition for the appearance of the peak is the existence of a proper phase relation between the position of the measuring magnetic probe and the O point of the slowly rotating dominant (1,7) mode, deduced by a magnetic field map reconstruction based on the determination of the mode eigenfunction from Newcomb's equation [13]. Indeed, the QSH phases produce internal transport barriers surrounding a broad portion of hot plasma, where the electron temperature T_e often exceeds 1 keV [13]. These barriers, being associated with the $m = 1$ helicity of the dominant mode, are typically asymmetric across the poloidal section. This is particularly true for the states characterized by a perturbation of the axisymmetric equilibrium. It has been proven [13] that strong T_e gradients can form, in such conditions, just on the poloidal side, where the O point of the (1,7) mode lies. An example is given in Fig. 2(b): two radial T_e profiles, taken on the equatorial plane evaluated at the same two time instants used for the power spectra in QSH phases of Fig. 2(a), are shown. They are both characterized by the presence of strong gradients, but while the black curve exhibits internal transport barriers on both the low- ($r < 0$) and the high-field side of the torus, the red one is strongly asymmetric, with a steep T_e gradient at $r > 0$ only. The toroidal position of the Thomson scattering diagnostics is such that the inboard midplane ($r < 0$) of the T_e profile almost corresponds to the position along the warped helical structure where the probes are placed. The high-frequency instability is thus observed when the steepest part of the gradient is close to the in-vessel magnetic probe.

The relation between the T_e gradient and the mode in a large variety of discharges is shown in Fig. 3, where A^* is plotted versus the normalized logarithmic temperature gradient $a/L_{T_e} = -ad(\log T_e)/dr$ at the barrier location for two intervals of the β parameter (ratio of thermal

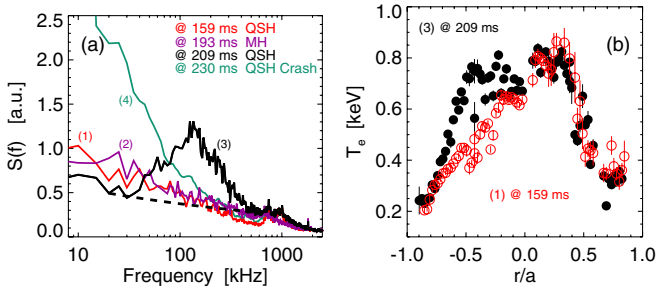

FIG. 2 (color online). (a) Power spectrum of a $\dot{b}_\theta$ signal evaluated at the four time instants indicated in Fig. 1. The dashed line is the interpolation as $f^{-\alpha}$ of the spectrum at 209 ms in the frequency region above and below that of the quasicoherent broad peak. (b) Electron temperature radial profiles measured at the time instants corresponding to the black and the red curve of frame (a).

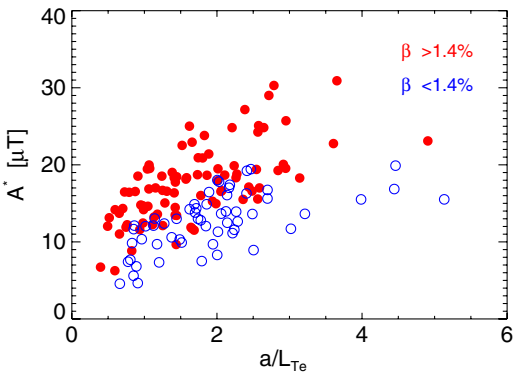

FIG. 3 (color online). Amplitude of the mode A^* vs the normalized logarithmic T_e gradient. Closed and open circles refer to high- and low-β values, respectively.

electronic pressure to the magnetic pressure). A clear increasing trend is found with a/L_{T_e}. Furthermore, lower β values are associated to lower amplitude of the instability.

By means of closely spaced coils at different toroidal and poloidal positions, and applying the two-point technique [19], we have estimated the (m, n) couples associated to the instability, up to $|m| \leq 16$ and $|n| \leq 350$. The technique is based on a statistical approach by dividing the signals into slices considered as independent realizations of the process under study.

In Fig. 4, where the $S(m, f)$ and $S(n, f)$ spectra are given as color-coded contours, the peak observed in the spectrum of Fig. 2(a) is now recognizable at extremely high m and n mode numbers. The $S(m)$ and $S(n)$ spectra are also shown, where $S(k) = \int S(k, f)df$, the integration being performed over the frequency range of the peak. Actually, the measured mode number m is close to the limit of the system, part of the spectrum being affected by aliasing. Nevertheless, the structure of the instability under study is clearly found to be centered, in this case, around $(m, n) = (15, 190)$, which suggests a resonant condition $q(r_{\rm res}) = m/n$ satisfied at $r_{\rm res}/a \approx 0.6$, i.e., in the region of the maximum T_e gradient [see Fig. 5(a) below]. Such large wave numbers (m, n), related to wavelengths in the centimetric range, force to address the kinetic problem of instabilities and turbulence with $k_y\rho_i \lesssim 1$ (k_y is the binormal wave number, orthogonal to the magnetic field line and tangent to the magnetic surface), i.e., within the

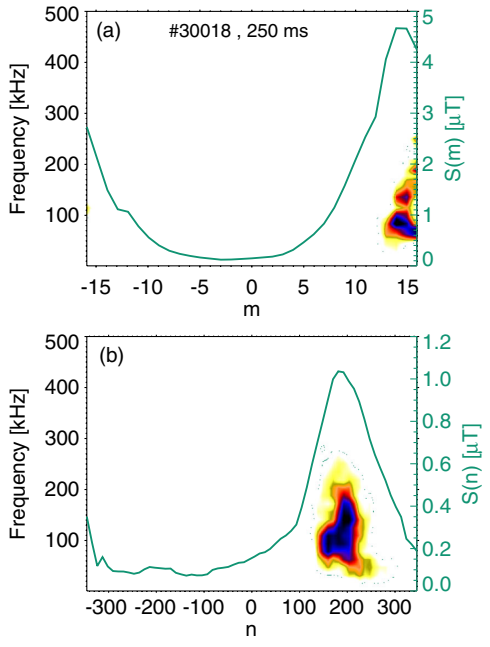

FIG. 4 (color online). (a) Color coded $S(m, f)$ spectrum (in a.u.) deduced by the two-point analysis using two magnetic coils poloidally separated. The right-hand side y axis refers to the $S(m)$ spectrum (continuous green line). (b) Same analysis as in (a) performed for the $S(n, f)$ spectrum.

gyrokinetic formalism [20]. To this aim we have used the flux-tube code GS2 [21] to look for the occurrence of microinstabilities in a subset of the experimental database investigated in the Letter.

The code GS2 can now deal with the RFP configuration [22]. The geometry takes into account the peculiar curvature and ∇B drifts, and the different role of the parallel dynamics with respect to tokamaks, due to the low value of q. However, whenever the problem of the coexistence of transport barriers and single helicity states is addressed, we have to keep in mind the underlying assumption of field axisymmetry. Indeed, the values of q, of magnetic shear $\hat{s} = (r/q)dq/dr$ and of the radial gradients considered are unrelated to the natural modifications provided by the helical deformation of the magnetic field. In this respect, we recall that RFP helical states are characterized by a flat (helical) q profile corresponding to the electron temperature barrier [1]. For the electron to ion temperature ratio, the value $T_e/T_i \simeq 3/2$ is assumed. An important role is played by the local values of collisionality and plasma β, especially for the electromagnetic instabilities we are going to investigate. Fluctuations in electrostatic potential ϕ and parallel vector potential $A_\parallel$ are included. $A_\perp$ fluctuations are neglected, as they only slightly modify the results.

In the analysis carried out in Ref. [23], discharges characterized by peaked T_e profiles were revealed to be prone to microtearing modes. Within the set of discharges investigated in this Letter, the presence of microtearing modes across electron temperature barriers is confirmed. The steep gradients are always located at midradius, usually in the range $0.4 \lesssim r/a \lesssim 0.6$, with a/L_{T_e} reaching values above $\sim$4, as shown in Fig. 5(a) in the considered shaded region. Microtearing modes are characterized by $A_\perp \sim 0$ or, equivalently, $b_\parallel \simeq 0$, which implies $b_\theta \simeq b_y/[1 + (r/R)^2/q^2]^{1/2}$, with b_y the binormal component of b. The poloidal component b_θ generated around midradius, where $b_\theta \sim b_y/\sqrt{2}$, has thus to be compared with b_θ measured at the edge.

In Fig. 5(b) the growth rate for the same shot of Fig. 4 as a function of the normalized wave number $k_y\rho_i$ is shown for several radii. Solid symbols represent the data set with the axisymmetric q profile of Fig. 5(a), while open symbols are obtained by artificially halving the magnetic shear, in an attempt to roughly model the flatter helical q profile; cf. Fig. 2 of Ref. [1]. This has to be understood as a parametric scan over one of the most sensitive (and less measurable) parameters. It is evident how slight changes in the q profile can affect the results.

All of the modes of Fig. 5(b) are identified as microtearing as their eigenfunctions have the peculiar odd symmetry in ϕ and even in $A_\parallel$, the latter being much more localized in the parallel direction than the former, and propagate in the electron diamagnetic direction; the estimate of the phase velocity is fully consistent with the

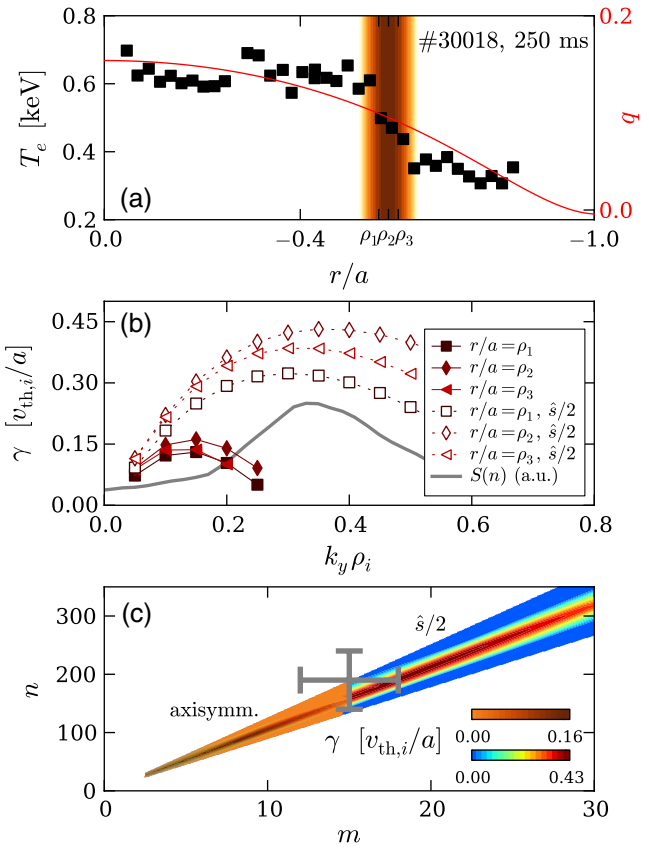

FIG. 5 (color online). For the shaded area of frame (a) the growth rates of the most unstable modes (all with microtearing parity) as a function of the wave number $k_y\rho_i$ are in (b), solid symbols; open symbols represent the same data set with q profile artificially flattened, $\hat{s} = \hat{s}_{\text{expt}}/2$; the gray line is the spectrum $S(n)$ of Fig. 4; in (c) the γ spectra are exploded on the (m, n) plane, with the experimental estimate of the measured wave numbers at the edge (gray error bars).

corresponding experimental values derived from the dispersion relation of the $S(n, f)$ spectrum, $v_p \sim 10^4$ m/s. Another hallmark of the microtearing mode is its dependence on some parameters of the plasma: in particular, as shown in Refs. [23,24], the growth rate gets larger for higher values of a/L_{T_e} and β, consistently with the results shown in Fig. 3. In Fig. 5(c) we show the same growth rates in the (m, n) plane evaluated at different radii, both for the axisymmetric and halved-shear case, where the poloidal and toroidal wave numbers are given by $n = rk_y/[(r/R)^2 + q^2]^{1/2}$ and $m = qn$. This relation allows us to compare the gyrokinetic linear spectra with the measured $S(n(k_y))$ spectrum at the edge, gray solid line of Fig. 5(b), exhibiting good agreement. The experimental peak in the (m, n) plane is shown as deduced from Fig. 4, with the error bars evaluated as the FWHM of the bell shaped $S(m)$ and $S(n)$ spectra.

Up to this stage we can claim that all evidences point towards our interpretation of magnetic fluctuations as due to the microtearing modes. Nonetheless, a few points are not easily framed inside the picture: (i) Simulation and experiment yield mutually consistent ratios m/n but the individual figures for the wave numbers do overlap only in the halved-shear case. We do not think this issue to be serious since, as mentioned above, such a flattening of the q profile is naturally provided in helical states. Furthermore, while flat q profiles destabilize the mode toward large values of (m, n), an opposite shrinking of the spectrum at low wave numbers is expected in a nonlinear framework [5]. A quantitative evaluation of the resulting spectrum requires 3D nonlinear studies, largely beyond the scope of the present work as well as present computing capabilities. (ii) The experimental uncertainties do not allow us to identify a critical a/L_{T_e} value as would be theoretically expected for the stability of microtearing modes. (iii) Microtearing modes quasilinearly saturate for magnetic field perturbations reaching $b_r/B \sim \rho_e/L_{T_e}$ [8], this claim being supported by nonlinear simulations [5]. For our plasmas, this relation yields $b_r \sim 0.1$–1 mT at the mode resonances. The amplitude of the measured $b_\theta(a)$ signals is a factor 10^{-4}–10^{-3} smaller than this. While in a slab geometry the b_r and b_y components would be comparable, decaying as $\sim \exp(-k_y|x|)$ for $|x| \gg \rho_i$ (x is the radial coordinate centered at the resonance), and would provide an almost negligible signal $b_y(a)$, in a nonlinear toroidal framework the picture is rather different. According to [5], the $A_\parallel$ perturbations are very broad in the radial direction of a tokamak, especially on the outboard side of the torus. Because of the similar ballooning structure of the $A_\parallel(\theta)$ eigenfunctions in the RFP, we expect the same result to hold in the present scenario. If, on the one hand, this implies $b_y/b_r \sim k_r/k_y \ll 1$, on the other hand it drags a large-scale $A_\parallel(r)$ perturbation close to the edge. Thus we expect the measured $b_\theta(a)$ to be the signature of a well-extended $A_\parallel(r)$ envelope. Again, a quantitative evaluation would require full-torus nonlinear simulations.

Summarizing, we have been able to provide an extensive experimental investigation of electromagnetic microscopic modes in RFX-mod. All evidence points to identifying them with good confidence as microtearing modes, representing therefore the first direct observation ever of these modes in a laboratory plasma.

We are grateful to X. Garbet, F. Zonca, and L. Carraro for helpful discussions and to the referees for their valuable comments. This work was supported by EURATOM and carried out within the framework of the European Fusion Development Agreement.

[1] M. Gobbin, D. Bonfiglio, D. Escande, A. Fassina, L. Marrelli, A. Alfier, E. Martines, B. Momo, and D. Terranova, Phys. Rev. Lett. **106**, 025001 (2011).
[2] R. Lorenzini *et al.*, Nucl. Fusion **52**, 062004 (2012).

[3] X. Garbet, Y. Idomura, L. Villard, and T. H. Watanabe, Nucl. Fusion **50**, 043002 (2010), and refs. therein.
[4] K. L. Wong, S. Kaye, D. Mikkelsen, J. Krommes, K. Hill, R. Bell, and B. LeBlanc, Phys. Rev. Lett. **99**, 135003 (2007).
[5] W. Guttenfelder, J. Candy, S. Kaye, W. Nevins, E. Wang, R. Bell, G. Hammett, B. LeBlanc, D. Mikkelsen, and H. Yuh, Phys. Rev. Lett. **106**, 155004 (2011); H. Doerk, F. Jenko, M. J. Pueschel, and D. R. Hatch, Phys. Rev. Lett. **106**, 155003 (2011).
[6] J. Kesner and S. Migliuolo, Nucl. Fusion **39**, 163 (1999); Y. T. Lau, Nucl. Fusion **30**, 934 (1990); K. McGuire *et al.*, Plasma Phys. Controlled Nucl. Fusion Res. **1**, 117 (1985).
[7] R. D. Hazeltine, D. Dobrott, and T. S. Wang, Phys. Fluids **18**, 1778 (1975).
[8] J. F. Drake, N. T. Gladd, C. S. Liu, and C. L. Chang, Phys. Rev. Lett. **44**, 994 (1980).
[9] P. Martin *et al.*, Nucl. Fusion **51**, 094023 (2011).
[10] N. Vianello, M. Spolaore, E. Martines, R. Cavazzana, G. Serianni, M. Zuin, E. Spada, and V. Antoni, Nucl. Fusion **50**, 042002 (2010).
[11] M. Zuin, S. Spagnolo, R. Paccagnella, E. Martines, R. Cavazzana, G. Serianni, M. Spolaore, and N. Vianello, Nucl. Fusion **50**, 052001 (2010).
[12] R. Paccagnella *et al.*, Phys. Rev. Lett. **97**, 075001 (2006).
[13] R. Lorenzini *et al.*, Nat. Phys. **5**, 570 (2009).
[14] P. Piovesan *et al.*, Nucl. Fusion **49**, 085036 (2009).
[15] R. Lorenzini, D. Terranova, A. Alfier, P. Innocente, E. Martines, R. Pasqualotto, and P. Zanca, Phys. Rev. Lett. **101**, 025005 (2008).
[16] D. F. Escande, R. Paccagnella, S. Cappello, C. Marchetto, and F. DAngelo, Phys. Rev. Lett. **85**, 3169 (2000).
[17] S. Spagnolo, M. Zuin, F. Auriemma, R. Cavazzana, E. Martines, M. Spolaore, and N. Vianello, Nucl. Fusion **51**, 083038 (2011).
[18] M. Zuin, N. Vianello, M. Spolaore, V. Antoni, T. Bolzonella, R. Cavazzana, E. Martines, G. Serianni, and D. Terranova, Plasma Phys. Controlled Fusion **51**, 035012 (2009).
[19] J. M. Beall, Y. C. Kim, and E. J. Powers, J. Appl. Phys. **53**, 3933 (1982).
[20] A. J. Brizard and T. S. Hahm, Rev. Mod. Phys. **79**, 421 (2007).
[21] M. Kotschenreuther, G. Rewoldt, and W. M. Tang, Comput. Phys. Commun. **88**, 128 (1995); W. Dorland, F. Jenko, M. Kotschenreuther, and B. N. Rogers, Phys. Rev. Lett. **85**, 5579 (2000).
[22] I. Predebon, C. Angioni, and S. C. Guo, Phys. Plasmas **17**, 012304 (2010).
[23] I. Predebon, F. Sattin, M. Veranda, D. Bonfiglio, and S. Cappello, Phys. Rev. Lett. **105**, 195001 (2010).
[24] D. J. Applegate, C. M. Roach, J. W. Connor, S. C. Cowley, W. Dorland, R. J. Hastie, and N. Joiner, Plasma Phys. Controlled Fusion **49**, 1113 (2007).